analytical chemistry

Article

pubs.acs.org/ac

Porphyrin-Encapsulated Metal–Organic Frameworks as Mimetic Catalysts for Electrochemical DNA Sensing via Allosteric Switch of Hairpin DNA

Pinghua Ling, Jianping Lei,* Lei Zhang, and Huangxian Ju

State Key Laboratory of Analytical Chemistry for Life Science, School of Chemistry and Chemical Engineering, Nanjing University, Nanjing 210093, People's Republic of China

ABSTRACT: A sensitive electrochemical sensor is designed for DNA detection based on mimetic catalysis of metal–organic framework (MOF) and allosteric switch of hairpin DNA. The functional MOFs are synthesized as signal probes by a one-pot encapsulation of iron(III) meso-5,10,15,20-tetrakis(4-carboxyphenyl) porphyrin chloride (FeTCPP) into a prototypal MOF, HKUST-1(Cu), and sequentially conjugated with streptavidin (SA) as a recognition element. The resulting FeTCPP@MOF composites can mimetically catalyze the oxidation of *o*-phenylenediamine (*o*-PD) to 2,2′-diaminoazobenzene, which is a good electrochemical indicator for signal readout. The presence of target DNA introduces the allosteric switch of hairpin DNA to form SA aptamer, and thus, FeTCPP@MOF-SA probe is brought on the electrode surface via the specific recognition between SA and the corresponding aptamer, resulting in the enhancement of electrochemical signal. The "signal-on" electrochemical sensor can detect target DNA down to 0.48 fM with the linear range of 10 fM to 10 nM. Moreover, the MOF-based electrochemical sensor exhibits acceptable selectivity against even a single mismatched DNA and good feasibility in complex serum matrixes. This strategy opens up a new direction of porphyrin-functionalized MOF for signal transduction in electrochemical biosensing.

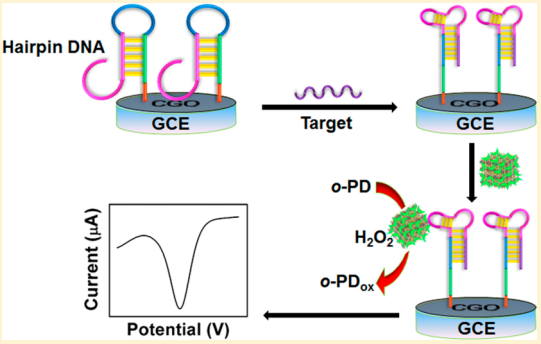

Metal–organic frameworks (MOFs) are crystalline molecular materials that possess unique physical and chemical properties with an unprecedentedly large and permanent inner porosity.[1−7] Functional MOFs have shown versatile applications in gas drug delivery,[8−10] gas storage,[11] cancer therapy,[12,13] and optical imaging.[14−16] In particular, the exceptional tunability of MOF structures and properties would constitute an important advantage over other conventional chemo-sensory materials in biosensing.[17−21] To realize the specific functions of porous MOFs, there are three different strategies to modify MOFs easily: dopant modification,[22] postsynthesis methods,[23,24] and entrapping functional molecules or nanoparticles within the framework.[25−27] For example, a simple, color-changing, ratiometric oxygen sensor was constructed by doping small amounts of Ru^{II} in an ultramicroporous, fluorescent Zn^{II} coordination polymer.[28] A nanocomposite material consisting of azobenzene-functionalized graphene oxide and stilbene-MOF displayed selectivity to dinitrotoluene over trinitrotoluene with subppm sensitivity.[29] Alternatively, entrapping of functional molecules in MOF materials is a promising method for the design of functional MOFs and signal-transduction strategy.

As the active center of heme proteins, iron porphyrins are widely applied as mimetic molecules to catalytic oxidation such as hydroxylation and epoxidation of hydrocarbons.[30,31] In order to overcome the μ-oxide dimers formed via the oxygen bridge (hindered access to catalytic sites)[32] and self-degradation of porphyrins due to the strong oxidation of high-valent porphyrin,[33] the immobilization of metalloporphyrins in solid matrices,[34−36] such as sol–gels,[37] synthetic zeolites,[38] and polymer films[39] can enhance their catalytic activity. However, in these systems, some disadvantages such as the low loading capacity, nonuniform distribution, and leakage of the catalyst molecules limit their applications in practice. Due to the tunable pore voids and functional pore walls, MOF provides a new opportunity for mimetic catalysis. In fact, a series of iron porphyrin derivatives can be readily functionalized as suitable components for the construction of MOFs and they show interesting peroxidase activity comparable to that of the heme protein.[40−46] As a MOF prototype, HKUST-1(Cu) possesses suitably sized and shaped cavities for entrapping anions,[47] a series of porphyrin-encapsulated MOFs were prepared using a template method and postsynthetic metal exchange,[48,49] while the remaining cavities allow small molecules to reach the active site for catalysis much like channels in heme proteins. In this work, a new type of porphyrin-encapsulated MOF material was achieved through a one-pot incorporation of porphyrin into the cage of HKUST-1(Cu) as catalyst, affording an efficient signal-transduction platform for DNA detection.

Received: January 1, 2015
Accepted: March 5, 2015
Published: March 5, 2015

DOI: 10.1021/acs.analchem.5b00001
Anal. Chem. 2015, 87, 3957−3963

Among the detection methods for DNA, an electrochemical sensor has unique and attractive strengths, including high sensitivity, low cost, simplicity, and portability.[50−52] In order to realize the signal readout, many DNA biosensors were based on the target-induced conformational switch via circular strand-replacement DNA polymerization and "Y" junction structure.[53−55] Typically, an "off-on" electrochemiluminescent (ECL) strategy was designed for highly sensitive and selective detection of 5′-triphosphate via duplex−aptamer conjugate structure switch.[56] A triplex-helix molecular beacon was designed as both a recognition element and a signal probe based on its dissemination after the formation of an aptamer/target duplex.[57] Herein, coupling with mimetic catalysis of porphyrin-encapsulated MOF as a signal probe, a label-free electrochemical strategy for DNA detection was designed through the allosteric switch of hairpin DNA (Scheme 1). The

Scheme 1. (A) Synthesis of FeTCPP@MOF-SA Composite and (B) Electrochemical DNA Sensing via Allosteric Switch of Hairpin DNA

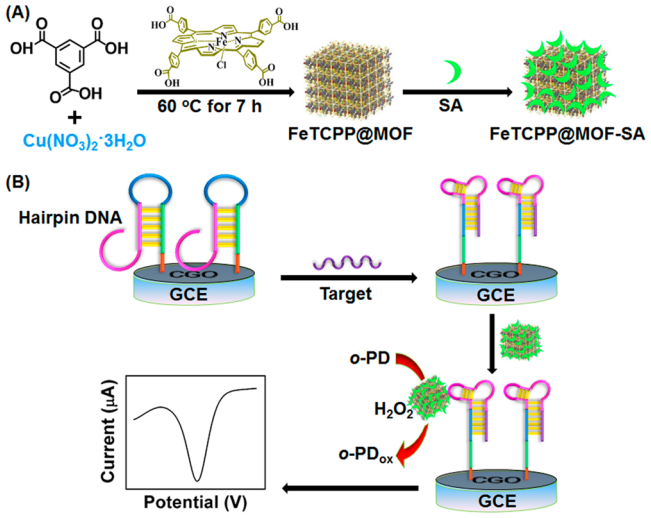

signal probes are synthesized by a one-pot encapsulation of iron(III) meso-5,10,15,20-tetrakis(4-carboxyphenyl) porphyrin chloride (FeTCPP) in the octahedral cage of a prototypal MOF, HKUST-1(Cu), and then conjugated with streptavidin (SA) as a recognition element. Initially, the SA aptamer sequence of a hairpin DNA was inaccessible owing to its loop structure.[58] Upon the addition of target DNA, the loop bound to the target sequence and thus the stem of hairpin DNA was unfolded to form a structure with the combinative SA aptamer. The activated hairpin DNA can selectively bind FeTCPP@MOF-SA via biorecognition affinity between SA aptamer and SA and then was utilized as mimetic catalyst to greatly enhance peroxidase activity toward *o*-phenylenediamine (*o*-PD) oxidation in the presence of H_2O_2. Thus, the detectable electrochemical signal was generated from the oxidized product (*o*-PD_{ox}).[45,59] The "signal-on" electrochemical sensor demonstrates a good performance for DNA detection with a detection limit down to 0.48 fM, the 6-order magnitude linear range, single mismatch differentiation ability, and practical application in complex samples. The functionalized MOF offers an excellent signal transduction platform for detecting a wide range of the analysts and significantly demonstrates a proof-of-concept for biosensing applications.

EXPERIMENTAL SECTION

Materials and Reagents. Copper nitrate ($Cu(NO_3)_2 \cdot 3H_2O$), 1,3,5-benzene-tricarboxylic acid (H_3BTC), ethanol, dimethylformamide (DMF), streptavidin (SA), 1-(3-(dimethylamino)propyl)-3-ethylcarbodiimide hydrochloride (EDC, purity ≥98%), *N*-hydroxysuccinimide (NHS), and horseradish peroxidase (HRP) were purchased from Sigma-Aldrich Inc. (U.S.A.). FeTCPP was obtained J&K Scientific Ltd. (China). *o*-Phenylenediamine and tris(hydroxy-methyl)-aminomethane-HCl (Tris-HCl) were obtained from Sunshine Biotechnology Co., Ltd. (Nanjing, China). Hydrogen peroxide (H_2O_2) was purchased from Ling Feng Chemical Reagent Co., Ltd. (Shanghai, China). Carboxylic graphene oxide (CGO, purity > 99.8%, carboxyl ratio > 5.0 wt %, single layer ratio > 80%) was purchased from Nanjing XFNano Materials Tech Co. Ltd. (Nanjing, China). In our work, 0.1 M phosphate buffer saline (PBS) at various pH values were prepared by mixing stock standard solutions of Na_2HPO_4, KH_2PO_4, NaCl, or KCl and then adjusted to the required pH value using 0.1 M HCl or NaOH. Ultrapure water obtained from a Millipore water purification system (Milli-Q, ≥18.2 MΩ) was used throughout the experiments. Human serum samples were generously provided by Jiangsu Province Tumor Hospital. All DNA oligonucleotides were synthesized by Sangon Inc. (Shanghai, China). The sequences of DNA oligonucleotides are given below:

Hairpin DNA: 5′-**ATTGACCGCTGTGTGACGCA-ACACTCAATT**TCTCCAGTGTA-GTATTAGG-CAATGAAATTGAGTGTTTTTTTTTTTT-$(CH_2)_3$-SH-3′

Target DNA: 5′-CATTGCCTAATACTACACTG-GAGAA-3′

One-mismatched DNA: 5′-CATTCCCTAATACTAC-ACTGGAGAA-3′

Two-mismatched DNA: 5′-CATTGCCTAATAGTAC-ACTCGAGAA-3′

Three-mismatched DNA: 5′-CATTCCCTAATAGTAC-ACTCGAGAA-3′

Random DNA: 5′-CATACGGTATAAGATCACACCT-CAA-3′

The bold letters represent the SA aptamer sequence. The mismatched bases are underlined.

Apparatus. Scanning electron microscope (SEM) images were obtained using an S-4800 scanning electron microscope (Hitachi, Japan). X-ray diffraction (XRD) was determined through a Cu sealed tube (λ = 1.54178 Å) at 40 kV and 40 mA to found the crystal structures of the MOF. UV−vis spectra were recorded on a UV-3600 UV−vis-NIR spectrophotometer (Shimadzu Co., Kyoto, Japan). The nitrogen isotherms of HKUST-1(Cu) and FeTCPP@MOF were obtained on an automatic volumetric sorption analyzer (Micromeritics ASAP2020) at 77 K. Infrared spectra were observed on a Vector 22 Fourier transform infrared spectrometer (Bruker Optics, Germany). Electrochemical experiments, including cyclic voltammetry (CV) and differential pulse voltammograms (DPV), were conducted on CHI 660D electrochemical workstation (Shanghai CH Instruments, China) with a three-electrode system consisting of a glassy carbon electrode (GCE) as working electrode, a saturated calomel electrode (SCE; caution: it is toxic) as reference electrode, and platinum wire as counter electrode, respectively.

DOI: 10.1021/acs.analchem.5b00001
Anal. Chem. 2015, 87, 3957−3963

Preparation of HKUST-1(Cu) and FeTCPP@MOF. The HKUST-1(Cu) was synthesized according to a previous report.[60] First, 0.875 g (3.6 mM) of $Cu(NO_3)_2{\cdot}6H_2O$ was dissolved in 12 mL of deionized water and 0.42 g (2.0 mM) of H_3BTC was also dissolved in 12 mL of ethanol. Then the solutions were mixed before it was introduced in a Teflon liner that was then placed in an autoclave. The autoclave was heated at 120 °C for 12 h, followed by slowly cooling to room temperature. A blue powder was obtained via centrifugation and washed with water and DMF, and finally dried under vacuum at 80 °C for 24 h for further use.

The preparation of FeTCPP@MOF was performed according to previous method with some modifications.[21] In our work, 0.5 g H_3BTC and 30 mg of FeTCPP were dissolved in a mixture solution with 15 mL of 1:1 (v/v) ethanol and DMF, and then mixed with 7.5 mL of $Cu(NO_3)_2{\cdot}6H_2O$ (1.04 g) aqueous solution. The mixture was sonicated to ensure homogeneity and finally sealed in a 50 mL Teflon liner. The Teflon liner was placed into an autoclave and heated at 60 °C for 7 h, then allowed to cool to room temperature. The crystalline material was collected by centrifugation, and washed extensively with ethanol. After drying under vacuum at 60 °C for 12 h, FeTCPP@MOF nanocomposite was obtained.

Catalysis Study. FeTCPP and HKUST-1(Cu) were dissolved in ethanol, and HRP and FeTCPP@MOF were dissolved in PBS (50 mM, pH 6.5) and deionized water, respectively. Next, 5.0 μL of each of the three solutions (at 1.0 mg L^{-1}) was added to a cell containing 10 mM *o*-PD and 8.0 mM H_2O_2 in 5.0 mL of 0.1 M pH 7.4 nitrogen-saturated PBS. The reactions were then monitored by DPV at different times.

Bioconjugation of FeTCPP@MOF with SA. Covalent coupling of FeTCPP@MOF with SA was followed by standard carbodiimide chemistry using EDC and NHS. Briefly, 500 μL of 1 mg mL^{-1} FeTCPP@MOF aqueous solution was mixed with 200 μL of 400 mM EDC and 100 mM NHS in ultrapure water and reacted for 20 min at room temperature. The resulting mixture was centrifuged at 10,000 rpm for 20 min and washed several times with 25 mM PBS buffer (pH 7.4) containing 25 mM NaCl to remove excessive EDC and NHS. The precipitate was then redispersed in 200 μL ultrapure water with the addition of 0.5 mg mL^{-1} SA (200 μL), and reacted for 4 h at room temperature. After washing three times at 10000 rpm for 10 min to remove the unbound SA with PBS, the FeTCPP@MOF-SA obtained was stored at 4 °C for further use.

Construction and Electrochemical Detection of Biosensor. Prior to use, the GCEs were polished with a slurry of alumina oxide powder (1.0 and 0.05 μm) on chamois leather, washed ultrasonically and dried at room temperature. Then, 5 μL of CGO suspension (1 mg mL^{-1}) was applied on the GCE and dried in air, followed by 20 μL of 400 mM EDC and 20 μL of 100 mM NHS cast onto the GCE surface for 30 min. After being washed using 0.1 M pH 7.4 PBS, the electrode was exposed to 1 μM hairpin DNA in 25 mM Tris-HCl buffer (pH 7.4) containing 120 mM NaCl and 5 mM KCl for 4 h. The hairpin DNA-modified electrode was then incubated with different concentrations of DNA at optimized conditions. The biosensor was then used in CV and DPV (a pulse amplitude of 50 mV and a width of 50 ms) in 0.1 M pH 7.4 nitrogen-saturated PBS containing 10 mM *o*-PD and 8.0 mM H_2O_2, which was deaerated thoroughly with highly pure nitrogen for 15 min and maintained in a nitrogen atmosphere.

RESULTS AND DISCUSSION

Characterization of FeTCPP@MOF and FeTCPP@MOF-SA. The SEMs images of HKUST-1(Cu) and FeTCPP@MOF show a typical truncated octahedral geometry and crystal structure (Figure 1A,B),[61] which indicates the porphyrin did not affect the octahemioctahedral crystal structure due to the hydrophobic interactions between porphyrin and organic ligands in HKUST-1(Cu) framework. After modified with SA, the surface of FeTCPP@MOF-SA displays agglomerates (Figure 1C), illustrating that the SA protein was loaded on the FeTCPP@MOF crystallites. The crystal structure of HKUST-1(Cu) and FeTCPP@MOF was determined using powder XRD (Figure 1D). The XRD curves show the peaks at 11.8, 13.48, 14.84, 17.64, 19.16, and 20.38 degrees, which can be indexed to (222), (400), (331), (333), (420), and (442) of the octahedral geometry (JCPDF card number: 36−1452), indicating the octahemioctahedral crystal structure of MOF materials.[61,21]

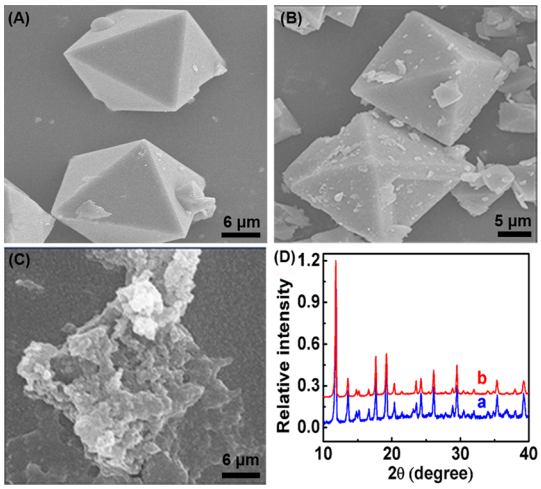

Figure 1. SEM images of (A) HKUST-1(Cu), (B) FeTCPP@MOF, and (C) FeTCPP@MOF-SA. (D) Powder X-ray diffraction patterns for HKUST-1(Cu) (a) and FeTCPP@MOF (b).

The encapsulation of FeTCPP in HKUST-1(Cu) was also confirmed by FT-IR and UV−vis absorption spectra. In the fingerprint region of IR spectra (Figure 2A), the peak at 1004 cm^{-1}, assigned to C−H bending vibrations of pyrrole rings,[62] could be observed for both FeTCPP (curve a) and FeTCPP@MOF (curve b), but not for HKUST-1(Cu) (curve c), identifying the successful encapsulation of porphyrin in the cages of HKUST-1(Cu). From the UV−vis spectra (Figure 2B), the maximum Soret absorption of FeTCPP in ethanol

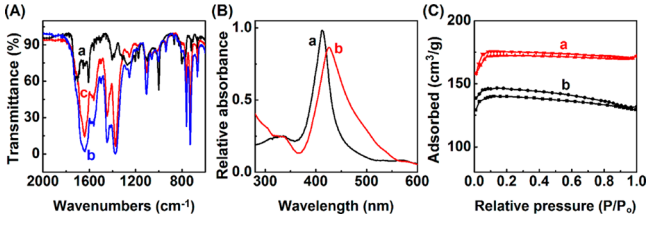

Figure 2. (A) FT-IR spectra for FeTCPP (a), FeTCPP@MOF (b), and HKUST-1(Cu) (c). (B) UV−vis absorption spectra of FeTCPP (a) and FeTCPP@MOF (b). (C) N_2 adsorption isotherms for HKUST-1(Cu) (a) and FeTCPP@MOF (b) at 77 K.

DOI: 10.1021/acs.analchem.5b00001
Anal. Chem. 2015, 87, 3957−3963

appeared at 412 nm (curve a), but it shifted to ~427 nm for FeTCPP@MOF (curve b). The 15 nm red shift could be contributed to the hydrophobic nature of the octahedral cavity and the sensitivity of the Soret band to the dielectric constant of the solvent.[63]

The nitrogen adsorption−desorption curves of HKUST-1(Cu) and FeTCPP@MOF nanostructure displayed type I isotherm (Figure 2C), which increases at low relative pressure (p/p_0 < 0.015), and reaches equilibrium at medium relative pressure and the high relative pressure (p/p_0 > 0.85), suggesting that micropores are dominant. The specific surface area of HKUST-1(Cu) and FeTCPP@MOF was estimated by the Brunauer−Emmett−Teller (BET) method to be 980 and 392 m^2 g^{-1}, respectively. The lower surface area of FeTCPP@MOF structure compared with pure HKUST-1(Cu) is also caused by the presence of porphyrin molecules in the HKUST-1(Cu) framework.

Mimetic Catalysis of FeTCPP@MOF. The CVs of 10 mM *o*-PD and 8.0 mM H_2O_2 at different electrodes in pH 7.4 nitrogen-saturated PBS are shown in Figure 3A. Both the bare

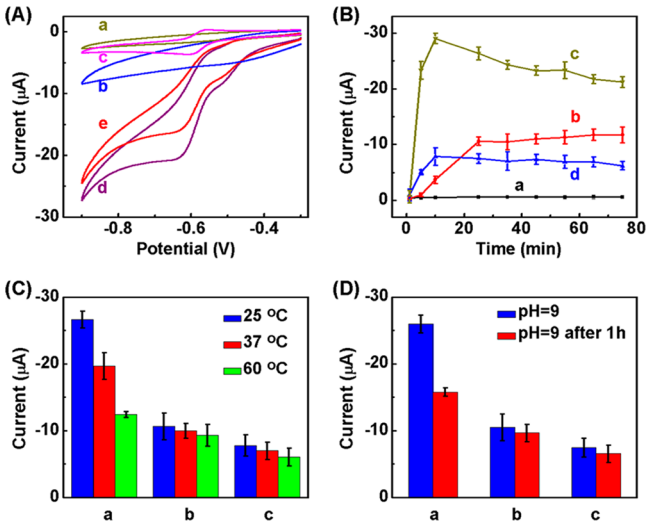

Figure 3. (A) CVs of bare GCE (a), HKUST-1(Cu)/GCE (b), FeTCPP/GCE (c), FeTCPP@MOF/GCE (d), and FeTCPP@MOF-SA/GCE (e). Scan rate: 50 mV s^{-1}. (B) Dependence of DPV response on the catalytic time for 1 mg mL^{-1} HKUST-1(Cu) (a), FeTCPP@MOF (b), HRP (c), and FeTCPP (d) in detection solution. Effects of (C) temperature for 0.5 h, and (D) alkaline conditions for 1 h on current intensity of *o*-PD/H_2O_2 reaction-catalyzed by HRP (a), FeTCPP@MOF (b), and FeTCPP (c). The detection solution is 0.1 M pH 7.4 nitrogen-saturated PBS containing 10 mM *o*-PD and 8.0 mM H_2O_2.

GCE (curve a) and HKUST-1(Cu)/GCE (curve b) showed no redox peaks, while a couple of well-defined redox peaks were observed from −0.3 and −0.9 V at FeTCPP/GCE (curve c). Comparing with FeTCPP/GCE (curve c), FeTCPP@MOF/GCE (curve d) showed a larger reduction peak at around −0.6 V, which corresponds to the electrochemical reduction of *o*-PD_{ox} formed by the catalytic oxidation of *o*-PD by FeTCPP in the presence of H_2O_2. The highly catalytic activity of FeTCPP@MOF could be explained that the loading of FeTCPP into the cage of HKUST-1(Cu) avoided the formation of bridged μ-oxide dimers (hindered access to catalytic sites) and oxidative self-degradation.[33] Moreover, the porous structure of HKUST-1(Cu) framework could accelerate the diffusion of *o*-PD in the electrochemical system.[64] When the FeTCPP@MOF-SA was immobilized on the GCE (curve e), the current response is slightly smaller than that of FeTCPP@MOF due to the inhibition of electron transfer by SA protein.

The catalytical properties of FeTCPP, HKUST-1(Cu), FeTCPP@MOF, and HRP (a commonly used natural catalyst) were studied by electrochemical measurements with the increasing time in the homogeneous reaction system (Figure 3B). The initial rate of oxidation of *o*-PD for FeTCPP@MOF was lower than that for HRP and FeTCPP, which was attributed to the slowing down of the diffusion of *o*-PD in and out of the channels of the framework after interacting FeTCPP@MOF via $\pi-\pi$ stacking. After 20 min, both FeTCPP and FeTCPP@MOF demonstrated quite stable catalytic ability than HRP, although HRP exhibited a high activity, indicating the minimal degradation of catalytic centers in the cage of MOF. In addition, compared with HRP, the mimetic catalyst of FeTCPP@MOF can sustain its stability and catalytic activity in broad conditions.[65] The effects of the temperature and pH on their catalytic activity in the same system were investigated as shown in Figure 3C and 3D. The catalytic activity of HRP was obviously vulnerable to high temperature, which demonstrates a 50% loss at 60 °C. However, FeTCPP@MOF was little affected by the temperature change (Figure 3C). When keeping HRP in pH 9.0 buffer for 1 h, HRP lost 39% of the catalytic activity, while FeTCPP@MOF displayed excellent stability (Figure 3D). Overall, the prepared FeTCPP@MOF catalyst exhibited much better stability than HRP with the change of time, temperature, and pH, showing the potential applications in broad fields.

Feasibility of the Sensor. After the electrochemical biosensor was constructed, the feasibility of the sensor was first investigated by conducting DPV in response to FeTCPP@MOF-SA and FeTCPP@MOF, and the results obtained are shown in Figure 4. Upon the addition of the target DNA, the

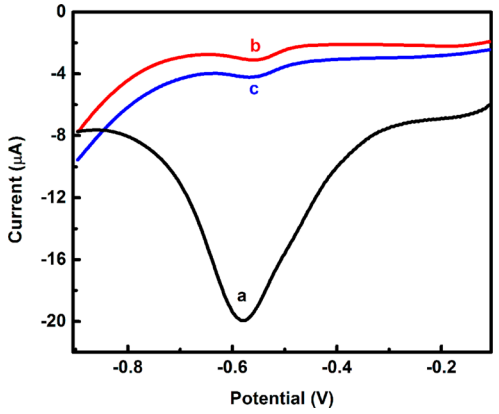

Figure 4. DPV responses of FeTCPP@MOF-SA (a, b) and FeTCPP@MOF (c) in the presence (a, c) and absence (b) of target DNA in the detection solution.

sensor showed a large peak current at −0.55 V (curve a), which should be corresponding to that the target DNA can induce the allosteric switch from the hairpin DNA to the SA aptamer, and then the latter could bind with FeTCPP@MOF-SA to catalytically oxidize *o*-PD to form *o*-PD_{ox} as detectable electrochemical indicator. In the absence of targets, the peak current decreases to 7% due to the nonspecific interaction

DOI: 10.1021/acs.analchem.5b00001
Anal. Chem. 2015, 87, 3957−3963

between the probes and the CGO via $\pi-\pi$ stacking (curve b). In addition, when using FeTCPP-HKUST-1(Cu) as signal probe, the catalytic current in the presence of target is similar to the blank (curve c), indicating the FeTCPP@MOF did not recognize SA aptamer.

Optimization of Detection Conditions. The pH of the electrolyte is an important factor relevant to DNA hybridization and the final electrochemical detection of target DNA. To obtain sufficient current, the influence of the solution pH on the response was investigated as shown in Figure 5A. In the

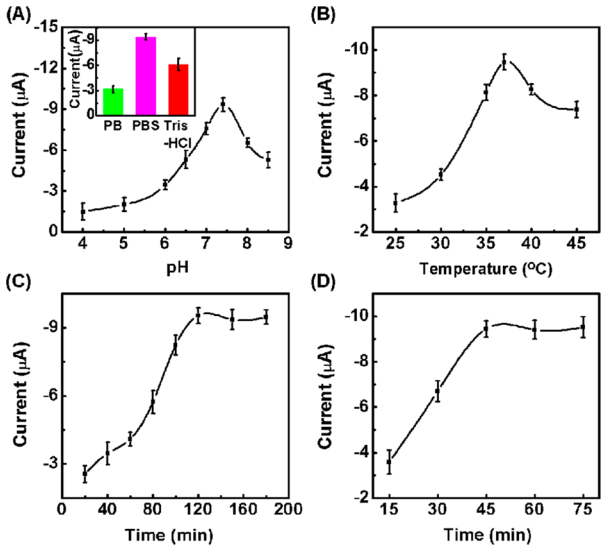

Figure 5. Effects of (A) pH and buffer type, (B) hybridization temperature, and (C) hybridization time between hairpin DNA and target, and (D) incubation time between SA aptamer and FeTCPP@MOF-SA on the electrochemical response.

examined pH range, the current reached the maximum value at pH 7.4. The category of buffer, including PBS, Tris-HCl, and phosphate buffer (PB, without NaCl and KCl), was also studied (inset in Figure 5A), which suggested that PBS had a more effective signal transduction capability than that of PB and Tris-HCl since PBS is more suitable for the hybridization of DNA than that of PB and Tris-HCl. Therefore, pH 7.4 PBS buffer was finally selected as the detection solution.

The effect of the hybridization temperature and time between hairpin DNA and target on the electrochemical response is shown in Figure 5B,C. The current signal increased gradually up to 37 °C and then rapidly declined at higher temperature (Figure 5B). Therefore, 37 °C was selected for the best hybridization temperature. At 37 °C, the current response increased with the increasing of hybridization time and then approached a constant value after 120 min (Figure 5C), so the optimal time was 120 min for the combination of hairpin DNA with target DNA. In addition, the incubation time between SA aptamer and FeTCPP@MOF-SA is an important parameter that influences the signal. After the incubation time for 45 min, the current signal increased and approached a platform (Figure 5D). Thus, 45 min was selected as the incubation time between SA aptamer and FeTCPP@MOF-SA.

Detection of Target DNA. Under the optimized conditions, different concentrations of target DNA were analyzed by the sensor with DPV measurements in 0.1 M pH 7.4 PBS. The peak current increased proportionally with the increasing concentration of target DNA in the range of 10 fM to 10 nM (Figure 6), which is wider than that of electrochemical DNA sensor using methylene blue-labeled

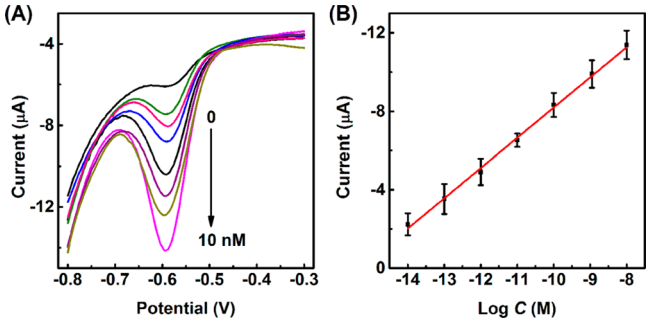

Figure 6. (A) DPV responses of FeTCPP@MOF-SA to different concentrations of target DNA at 0, 10 fM, 100 fM, 1 pM, 10 pM, 100 pM, 1 nM, and 10 nM (from up to down). (B) Calibration curve of current intensity vs logarithmic value of DNA concentration. The potential was at −0.55 V (vs Ag/AgCl).

DNA-Au nanoparticle as a signal probe (2.3 pM to 2.3 nM).[66] The detection limit was 0.48 fM at signal-to-noise ratio of 3 with a regression coefficient of 0.996 for seven points. The detection limit is much lower than that of Pt nanoparticle electrochemical amplification strategy (100 pM)[67] and electrochemical impedance spectroscopy (1 pM).[68] This excellent analytical performance can be ascribed to the good catalytic activity of FeTCPP in HKUST-1(Cu) microporous structure and the highly specific recognition between SA and the aptamer.

Selectivity of Sensor. To evaluate the robustness of the proposed method, several DNA sequences were tested, including complementary target DNA, single/two/three-base mismatched DNA, and a random DNA at the same concentrations (Figure 7). The signal of perfectly comple-

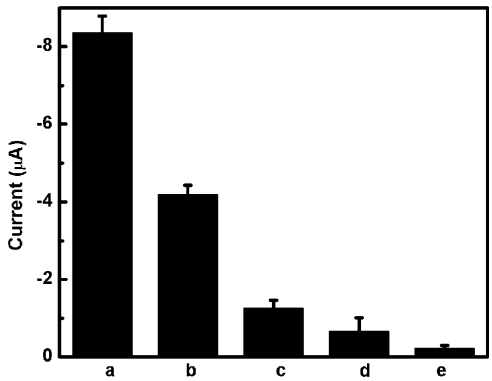

Figure 7. DPV response of FeTCPP@MOF-SA to 100 pM target DNA (a), single-base mismatched DNA (b), two-base mismatched DNA (c), three-base mismatched DNA (d), and random DNA (e) in the catalytic system of *o*-PD/H_2O_2.

mentary target was 2.1× that for single-base mismatched sequence, and the response to two/three-base mismatched strand was only 13% and 8.0% of that to perfectly complementary target, respectively. In addition, the random DNA produced a neglectable DPV signal. The high specificity of the biosensor is mainly due to specific dual biorecognition of DNA hybridization and the aptamer affinity.

DOI: 10.1021/acs.analchem.5b00001
Anal. Chem. 2015, 87, 3957−3963

Application in Complex Matrixes. To evaluate the universality of the proposed method in complex matrixes, clinical serum samples were further analyzed with the recovery test. By spiking standard target DNA solution (10 nM) into 10% (v/v) human serum samples, the recoveries were calculated to be 97.0 ± 1.3% (n = 3), suggesting the significant feasibility of the electrochemical strategy in practice.

CONCLUSIONS

This work designs a simple, sensitive, and flexible electrochemical method for biosensing based on mimetic catalysis of MOF and allosteric switch of hairpin DNA. The functional MOFs were synthesized via one-pot encapsulation of FeTCPP into a prototypal MOF and then bioconjugation with SA, which showed more efficient catalysis than FeTCPP and higher stability in broad conditions. The excellent catalytic activity should be contributed to the important features of FeTCPP@MOF material such as protecting the catalytic capacity of FeTCPP and the rapid diffusion of small molecules in the MOF cages. The introduction of target DNA triggered the unfolding of hairpin DNA and subsequent formation of free SA aptamer, leading to FeTCPP@MOF-SA was brought onto the electrode surface and generated the measurable electrochemical signal. The designed assay showed a detection range over 6 orders of magnitude with a detection limit of femtomolar level. Due to the dual biorecognition, the method could remarkably discriminate target DNA even from single-base mismatched oligonucleotide and complex matrixes. The present work provides a powerful tool to design sensitive biosensing strategies with multifunctional MOFs in bioanalysis.

AUTHOR INFORMATION

Corresponding Author

*Phone/Fax: +86-25-83593593. E-mail: jpl@nju.edu.cn.

Notes

The authors declare no competing financial interest.

ACKNOWLEDGMENTS

This work was financially supported by the National Basic Research Program of China (2010CB732400) and National Natural Science Foundation of China (21375060, 21135002, 21121091).

REFERENCES

(1) Li, H.; Eddaoudi, M.; O'Keeffe, M.; Yaghi, O. M. *Nature* **1999**, *402*, 276−279.
(2) Dinca, M.; Long, J. R. *Angew. Chem., Int. Ed.* **2008**, *47*, 6766−6779.
(3) Rosi, N. L.; Kim, J.; Eddaoudi, M.; Chen, B. L.; O'Keeffe, M.; Yaghi, O. M. *J. Am. Chem. Soc.* **2005**, *127*, 1504−1518.
(4) Lee, J.; Farha, O. K.; Roberts, J.; Scheidt, K. A.; Nguyen, S. T.; Hupp, J. T. *Chem. Soc. Rev.* **2009**, *38*, 1450−1459.
(5) Wang, Z. Q.; Cohen, S. M. *Chem. Soc. Rev.* **2009**, *38*, 1315−1329.
(6) Kitagawa, S.; Kitaura, R.; Noro, S. *Angew. Chem., Int. Ed.* **2004**, *43*, 2334−2375.
(7) Robson, R. *Dalton Trans.* **2008**, *38*, 5113−5131.
(8) Kathryn, M. L.; Pashow, T.; Rocca, J. D.; Xie, Z. G.; Tran, S.; Lin, W. B. *J. Am. Chem. Soc.* **2009**, *131*, 14261−14263.
(9) Horcajada, P.; Chalati, T.; Serre, C.; Gillet, B.; Sebrie, C.; Baati, T.; Eubank, J. F.; Heurtaux, D.; Clayette, P.; Kreuz, C.; et al. *Nat. Mater.* **2010**, *9*, 172−178.
(10) He, C. B.; Lu, K. D.; Lin, W. B. *J. Am. Chem. Soc.* **2014**, *136*, 12253−12256.
(11) Dinca, M.; Long, J. R. *Angew. Chem., Int. Ed.* **2008**, *47*, 6766−6779.
(12) Rieter, W. J.; Pott, K. M.; Taylor, K. M.; Lin, W. B. *J. Am. Chem. Soc.* **2008**, *130*, 11584−11585.
(13) He, C. B.; Lu, K. D.; Lin, W. B. *J. Am. Chem. Soc.* **2014**, *136*, 5181−5184.
(14) Rowe, M. D.; Thamm, D. H.; Kraft, S. L.; Boyes, S. G. *Biomacromolecules* **2009**, *10*, 983−993.
(15) Huxford, R. C.; Della, R. J.; Lin, W. B. *Curr. Opin. Chem. Biol.* **2010**, *14*, 262−268.
(16) Liu, D. M.; Huxford, R. C.; Lin, W. B. *Angew. Chem., Int. Ed.* **2011**, *50*, 3696−3700.
(17) Moulton, B.; Zaworotko, M. J. *Chem. Rev.* **2001**, *101*, 1629−1658.
(18) Yaghi, O. M.; O'Keeffe, M.; Ockwig, N. W.; Chae, H. K.; Eddaoudi, M.; Kim, J. *Nature* **2003**, *423*, 705−714.
(19) Perry, J. J., IV; Perman, J. A.; Zaworotko, M. J. *Chem. Soc. Rev.* **2009**, *38*, 1400−1417.
(20) O'Keeffe, M.; Yaghi, O. M. *Chem. Rev.* **2012**, *112*, 675−702.
(21) Larsen, R. W.; Wojtas, L.; Perman, J.; Musselman, R. L.; Zaworotko, M. J.; Vetromile, C. M. *J. Am. Chem. Soc.* **2011**, *133*, 10356−10359.
(22) Kreno, L. E.; Leong, K.; Farha, O. K.; Allendorf, M.; Van Duyne, R. P.; Hupp, J. T. *Chem. Rev.* **2012**, *112*, 1105−1125.
(23) Sun, F.; Yin, Z.; Wang, Q. Q.; Sun, D.; Zeng, M. H.; Kurmoo, M. *Angew. Chem., Int. Ed.* **2013**, *52*, 4538−4543.
(24) Morris, W.; Briley, W. E.; Auyeung, E.; Cabezas, M. D.; Mirkin, C. A. *J. Am. Chem. Soc.* **2014**, *136*, 7261−7264.
(25) Das, M. C.; Xiang, S. C.; Zhang, Z. J.; Chen, B. L. *Angew. Chem., Int. Ed.* **2011**, *50*, 10510−10520.
(26) Zhu, C. F.; Yuan, G. Z.; Chen, X.; Yang, Z. W.; Cui, Y. *J. Am. Chem. Soc.* **2012**, *134*, 8058−8061.
(27) Lei, J. P.; Qian, R. C.; Ling, P. H.; Cui, L.; Ju, H. X. *Trends Anal. Chem.* **2014**, *58*, 71−78.
(28) Qi, X. L.; Liu, S. Y.; Lin, R. B.; Liao, P. Q.; Ye, J. W.; Lai, Z. H.; Guan, Y. Y.; Cheng, X. N.; Zhang, J. P.; Chen, X. M. *Chem. Commun.* **2013**, *49*, 6864−6866.
(29) Lee, J. H.; Jaworski, J.; Jung, J. H. *Nanoscale* **2013**, *5*, 8533−8540.
(30) Beletskaya, I.; Tyurin, V. S.; Tsivadze, A. Y.; Guilard, R.; Stern, C. *Chem. Rev.* **2009**, *109*, 1659−1713.
(31) Collman, J. P.; Zhang, X. M.; Lee, V. J.; Uffelman, E. S.; Brauman, J. I. *Science* **1993**, *261*, 1404−1411.
(32) Guo, C. C.; Song, J. X.; Chen, X. B.; Jiang, G. F. *J. Mol. Catal. A: Chem.* **2000**, *157*, 31−40.
(33) Bell, S. E. J.; Hester, R. E.; Hill, J. N.; Shawcross, D. R.; Smith, J. R. L. *J. Chem. Soc., Faraday Trans.* **1990**, *86*, 4017−4023.
(34) Sacco, H. C.; Iamamoto, Y.; Lindsay Smith, J. R. *J. Chem. Soc., Perkin Trans.* **2001**, *2*, 181−190.
(35) Vinhado, F. S.; Prado-Manso, C. M. C.; Sacco, H. C.; Iamamoto, Y. *J. Mol. Catal. A* **2001**, *174*, 279−288.
(36) Li, Z.; Xia, C. G.; Zhang, X. M. *J. Mol. Catal. A* **2002**, *185*, 47−56.
(37) Battioni, P.; Cardin, E.; Louloudi, M.; Schöllhorn, B.; Spyroulias, G. A.; Mansuy, D.; Traylor, T. G. *Chem. Commun.* **1996**, 2037−2038.
(38) Holland, B. T.; Walkup, C.; Stein, A. *J. Phys. Chem. B* **1998**, *102*, 4301−4309.
(39) Nestler, O.; Severin, K. *Org. Lett.* **2001**, *3*, 3907−3909.
(40) Suslick, K. S.; Bhyrappa, P.; Chou, J. H.; Kosal, M. E.; Nakagaki, S.; Smithenry, D. W.; Wilson, S. R. *Acc. Chem. Res.* **2005**, *38*, 283−291.
(41) Goldberg, I. *Chem. Commun.* **2005**, 1243−1254.
(42) Farha, O. K.; Shultz, A. M.; Sarjeant, A. A.; Nguyen, S. T.; Hupp, J. T. *J. Am. Chem. Soc.* **2011**, *133*, 5652−5655.
(43) Burnett, B. J.; Barron, P. M.; Hu, C.; Choe, W. *J. Am. Chem. Soc.* **2011**, *133*, 9984−9987.
(44) Zou, C.; Zhang, Z.; Xu, X.; Gong, Q.; Li, J.; Wu, C. D. *J. Am. Chem. Soc.* **2012**, *134*, 87−90.
(45) Feng, D. W.; Gu, Z. Y.; Li, J. R.; Jiang, H. L.; Wei, Z. W.; Zhou, H. C. *Angew. Chem., Int. Ed.* **2012**, *51*, 10307−10310.

DOI: 10.1021/acs.analchem.5b00001
Anal. Chem. 2015, 87, 3957−3963

(46) Modak, A.; Nandi, M.; Mondal, J.; Bhaumik, A. *Chem. Commun.* **2012**, *48*, 248−250.
(47) Sun, C. Y.; Liu, S. X.; Liang, D. D.; Shao, K. Z.; Ren, Y. H.; Su, Z. M. *J. Am. Chem. Soc.* **2009**, *131*, 1883−1888.
(48) Zhang, Z. J.; Zhang, L. P.; Wojtas, L.; Nugent, P.; Eddaoudi, M.; Zaworotko, M. J. *J. Am. Chem. Soc.* **2012**, *134*, 924−927.
(49) Zhang, Z. J.; Zhang, L. P.; Wojtas, L.; Eddaoudi, M.; Zaworotko, M. J. *J. Am. Chem. Soc.* **2012**, *134*, 928−933.
(50) Fan, C. H.; Plaxco, K. W.; Heeger, A. J. *Proc. Natl. Acad. Sci. U.S.A.* **2003**, *100*, 9134−9137.
(51) Farjami, E.; Clima, L.; Gothelf, K.; Ferapontova, E. E. *Anal. Chem.* **2011**, *83*, 1594−1602.
(52) Xiao, Y.; Qu, X. G.; Plaxco, W. K.; Heeger, J. A. *J. Am. Chem. Soc.* **2007**, *129*, 11896−11897.
(53) Wang, Q.; Yang, L. J.; Yang, X. H.; Wang, K. M.; He, L. L.; Zhu, J. Q.; Su, T. Y. *Chem. Commun.* **2012**, *48*, 2982−2984.
(54) Shen, Z. L.; Nakayama, S.; Semancik, S.; Sintim, H. O. *Chem. Commun.* **2012**, *48*, 7580−7582.
(55) Hu, Y. H.; Xu, X. Q.; Liu, Q. H.; Wang, L.; Lin, Z. Y.; Chen, G. N. *Anal. Chem.* **2014**, *86*, 8785−8790.
(56) Liu, Y. T.; Lei, J. P.; Huang, Y.; Ju, H. X. *Anal. Chem.* **2014**, *86*, 8735−8741.
(57) Zheng, J.; Li, J. S.; Jiang, Y.; Jin, J. Y.; Wang, K. M.; Yang, R. H.; Tan, W. H. *Anal. Chem.* **2011**, *83*, 6586−6592.
(58) Song, Y. L.; Cui, L.; Wu, J.; Zhang, W. T.; Zhang, W. Y.; Kang, H. Z.; Yang, C. J. *Chem.—Eur. J.* **2011**, *17*, 9042−9046.
(59) Wang, Q. B.; Lei, J. P.; Deng, S. Y.; Zhang, L.; Ju, H. X. *Chem. Commun.* **2013**, *49*, 916−918.
(60) Chui, S. S. Y.; Lo, S. M. F.; Charmant, J. P. H.; Orpen, A. G.; Williams, I. D. *Science* **1999**, *283*, 1148−1150.
(61) Mao, J. J.; Yang, L. F.; Yu, P.; Wei, X. W.; Mao, L. Q. *Electrochem. Commun.* **2012**, *19*, 29−31.
(62) Feng, D. W.; Chung, W. C.; Wei, Z. W.; Gu, Z. Y.; Jiang, H. L.; Chen, Y. P.; Darensbourg, D. J.; Zhou, H. C. *J. Am. Chem. Soc.* **2013**, *135*, 17105−17110.
(63) Larsen, R. W.; Miksovska, J.; Musselman, R. L.; Wojtas, L. *J. Phys. Chem. A* **2011**, *115*, 11519−11524.
(64) Zhang, Y. F.; Bo, X. J.; Luhana, C.; Wang, H. A.; Li, M. A.; Guo, L. P. *Chem. Commun.* **2013**, *49*, 6885−6887.
(65) Gao, L. Z.; Zhuang, J.; Nie, L.; Zhang, J. B.; Zhang, Y.; Gu, N.; Wang, T. H.; Feng, J.; Yang, D. L.; Perrett, S.; Yan, X. Y. *Nat. Nanotechnol.* **2007**, *2*, 577−583.
(66) Cui, H. F.; Cheng, L.; Zhang, J.; Liu, R. H.; Zhang, C.; Fan, H. *Biosens. Bioelectron.* **2014**, *56*, 124−128.
(67) Kwon, S. J.; Bard, A. J. *J. Am. Chem. Soc.* **2012**, *134*, 10777−10779.
(68) Yang, Y. C.; Li, C.; Yin, L.; Liu, M. Y.; Wang, Z. X.; Shu, Y. Q.; Li, G. X. *ACS Appl. Mater. Interfaces* **2014**, *6*, 7579−7584.

DOI: 10.1021/acs.analchem.5b00001
Anal. Chem. 2015, 87, 3957−3963